Thermally Activated, Inverted Interfacial Electron Transfer Kinetics: High Driving Force Reactions between Tin Oxide Nanoparticles and Electrostatically-Bound Molecular Reactants

Dennis A. Gaal and Joseph T. Hupp*

Contribution from the Department of Chemistry, Northwestern University, 2145 Sheridan Road, Evanston, Illinois 60208-3113

Received July 7, 2000. Revised Manuscript Received September 6, 2000

Abstract: The kinetics and mechanism of fast electron transfer (ET) between tin oxide nanoparticles and electrostatically bound Os(III) and Ru(III) complexes have been examined via transient absorbance spectroscopy. Reaction-order studies establish that, at least in the short time regime, electrons are transferred directly from the tin oxide conduction band, rather than through localized redox trap states. The reactions occur in the high driving force regime ($\Delta G = -1.1$ to -2.3 eV) and span the Marcus normal region, barrierless region, and inverted region. (Inverted reactivity, while commonplace in homogeneous solution-phase reactions, has only rarely been observed in interfacial reactions.) Depending on the reactant, normal or inverted kinetic behavior can also be observed via pH-induced manipulation of the conduction band-edge energy and, therefore, the overall reaction driving force. The observation of kinetically resolved ET over such a wide range of driving forces permits the reorganization energy to be evaluated directly from the maximum of a log(rate constant) versus driving force plot. The value obtained, 1.4 eV, is much larger than expected based on solvent contributions alone. Further analysis of driving force effects suggests that significant, but not dominant, nonclassical contributions (high-frequency vibrational contributions) to the reorganization energy exist. Rate measurements in the barrierless region yield an estimated initial-state/final-state electronic coupling energy, H_{ab}, of 15−30 cm^{-1}, a value consistent with a moderately nonadiabatic ET pathway. Remarkably, even in the inverted region the reactions are thermally activated, with the activation effect evidently being amplified via an entropic driving force effect. Finally, the overall pattern of reactivity stands in remarkable contrast to the pH-independent, trapped-mediated kinetic behavior encountered for closely related metal complexes *covalently* bound to nanocrystalline TiO_2 surfaces.

Introduction

Surface modification of wide band gap semiconductor materials through attachment of sensitizing dyes offers the potential for visible-region photoelectrochemical applications[1] as well as interrogation of interfacial electron-transfer reaction kinetics. Electron transfer (ET) kinetics are often evaluated in terms of Marcus theory,[2,3] in which the rate of ET can be expressed for a nonadiabatic reaction in the classical activation limit as:

$$k_{ET} = (4\pi 2H_{ab}{}^2/h)(4\pi\lambda RT)^{-1/2} \exp[-\Delta G^*/RT] \qquad (1)$$

where

$$\Delta G^* = (\Delta G + \lambda)^2/4\lambda \qquad (2)$$

In the equations, ΔG^* is the activation free energy, H_{ab} is the coupling constant, and λ is the reorganization energy for the ET process. As a result, the log of the ET rate is a quadratic function with respect to the driving force. Initially, as the driving force increases, the rate of ET increases ("normal region kinetics"), reaching a maximum when the driving force equals the reorganization energy ($\Delta G^* = 0$). Beyond this, the rate decreases with increasing driving force ("inverted region kinetics").

For surface sensitization of semiconductors, most kinetic investigations have focused on sensitization by complexes covalently attached to TiO_2 surfaces through carboxylate[4−6] or phosphonate[7−9] linkages, primarily due to the interest in these systems for solar energy conversion.[10−12] In such systems, the two important interfacial ET processes are electron injection from the excited state of the dye into the semiconductor and back ET from the semiconductor to the oxidized species. In the case of excited-state injection, there is general agreement

* Author for correspondence. Fax: (847) 491-7713. E-mail: jthupp@chem.nwu.edu.

(1) Parkinson, B. A.; Spitler, M. T. *Electrochim. Acta* **1992**, *37*, 943−948.
(2) Marcus, R. A. *J. Chem. Phys.* **1965**, *43*, 679−701.
(3) Marcus, R. A.; Sutin, N. *Biochim. Biophys. Acta* **1985**, *811*, 265−322.
(4) Desilvestro, J.; Grätzel, M.; Kavan, L.; Moser, J.; Augustynski, J. *J. Am. Chem. Soc.* **1985**, *107*, 2988−2990.
(5) Nazeeruddin, M. K.; Kay, A.; Rodicio, I.; Humphry-Baker, R.; Muller, E.; Liska, P.; Vlachopoulos, N.; Grätzel, M. *J. Am. Chem. Soc.* **1993**, *115*, 6382−6390.
(6) Moser, J.; Punchihewa, S.; Infelta, P. P.; Grätzel, M. *Langmuir* **1991**, *7*, 3012−3018.
(7) Yan, S. G.; Hupp, J. T. *J. Phys. Chem.* **1997**, *101*, 1493−1495.
(8) Zaban, A.; Ferrere, S.; Gregg, B. A. *J. Phys. Chem. B* **1998**, *102*, 452−460.
(9) Bonhôte, P.; Moser, J.; Humphrey-Baker, R.; Vlachopoulos, N.; Zakeeruddin, S. M.; Walder, L.; Grätzel, M. *J. Am. Chem. Soc.* **1999**, *121*, 1324−1336.
(10) O'Regan, B.; Grätzel, M. *Nature* **1991**, *353*, 737−739.
(11) Hagfeldt, A.; Grätzel, M. *Chem. Rev.* **1995**, *95*, 49−68.
(12) Bach, U.; Lupo, D.; Comte, P.; Moser, J. E.; Weissörtel, F.; Salbeck, J.; Spreitzer, H.; Grätzel, M. *Nature* **1998**, *395*, 583−585.

10.1021/ja0024744 CCC: $19.00
Published on Web 10/21/2000

Scheme 1

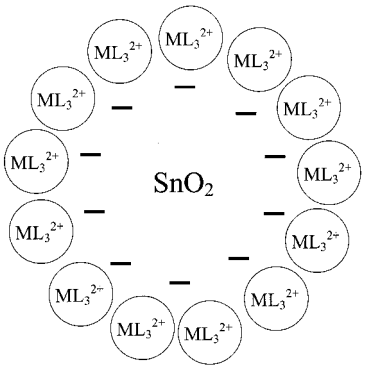

that the kinetic behavior is multiexponential and often on the femtosecond time scale due to excellent energy matching between the conduction band and the excited state of the dye.[13−16] However, in the case of the back ET, this consensus is lacking as widely differing behavior has been reported, with ET reaction times ranging from picoseconds to microseconds.[17−23] With regard to Marcus behavior, certain kinetic studies have shown that the back ET reaction for these types of systems is in the normal region,[24] while other systems show inverted behavior,[25,26] while even other studies indicate that the back ET process is roughly independent of the redox potential of the sensitizer and thereby indicate that Marcus kinetics are not applicable to these systems.[27,28]

In contrast to the extensive research on interfacial ET kinetics for the covalent-linked systems, mechanistic studies of the back ET process in systems utilizing electrostatic stabilization—for example, Coulombic binding of a cationic dye to a semiconductor featuring a net negative surface charge, such as colloidal SnO_2, as shown in Scheme 1, have been less completely investigated.[29−33] As a result, a systematic mechanistic understanding of back ET kinetics, including thermodynamic driving force effects, is currently lacking for these systems. Recently, in an effort to address this question, we examined the kinetics of back ET from collodial SnO_2 to a series of electrostatically attached ruthenium tris(polypyridyl) dyes featuring a modest range of redox potentials and, therefore, a modest range of driving forces.[34] On the basis of these preliminary studies, we found that back ET—for this family of systems—occurs in the Marcus inverted region and that the reactions are thermally activated. We have now extended and substantially expanded the study to encompass a very wide range of driving forces, extending from deeply inverted kinetic behavior to barrierless behavior to Marcus normal-region behavior. The expanded study provides sufficient information for direct evaluation of the reorganization energy and for estimation of the electronic coupling energy. The value found for the latter is broadly consistent with an expected weakly nonadiabatic reaction pathway. The former, on the other hand, is much larger than one would expect from conventional models of interfacial reactivity. Further mechanistic insight is provided by (a) laser power-dependence/electronic reaction-order studies, which indicate that electrons are transferred directly from the semiconductor's conduction band, rather than through surface states, (b) variable pH studies, which show that the back-reaction driving force can be systematically changed by varying the conduction band-edge energy and also show that the surface-bound dye is unaffected by putative interfacial redox-energy-coupling effects, and (c) variable-temperature kinetic studies, which indicate that the reorganization energy is dominated by classical modes.

Experimental Section

Materials. Colloidal SnO_2 (15 wt %) was purchased from Alfa and used as received. Average particle diameter was taken as 15 nm with a density of 6.95 g cm^{-3}.[35] 1,10-Phenanthroline and 1,10-phenanthroline derivatives were purchased from GFS Chemical Co. and used as received. $RuCl_3 \cdot 3H_2O$ was purchased from Aesar. All other chemicals were purchased from Aldrich Chemical Co. and used as received. Water was purified by a Milli-Q purification system to a resistivity of 15 MΩ or greater.

All ruthenium[36] and osmium[37] complexes were prepared by modifications to published methods. For the ruthenium tris-phenanthroline derivatives, $RuCl_3 \cdot 3H_2O$ was reacted with 3 equiv of the appropriate ligand in N_2 degassed ethylene glycol for 3−4 h, in which time the solution turned orange. Upon cooling, a saturated aqueous solution of NH_4PF_6 was added, causing the precipitation of the ruthenium complex which was isolated by filtration and washed with H_2O and ether. Purity was confirmed by ^1H NMR and by comparison of electrochemical responses to literature reports.[38] The PF_6^- salt was converted to the Cl^- salt by dissolution in acetone and addition of a concentrated solution of tetrabutylammonium chloride. The product was filtered and washed with acetone and ether and recrystallized from acetonitrile/ether. Typical yields were 70−80% based on starting material.

The osmium tris-phenanthroline and bis-phenanthroline adducts were synthesized by reaction of *cis*-$Os(L)_2Cl_2$[37] (where L = phenanthroline

(13) Hannappel, T.; Burfeindt, B.; Storck, W.; Willig, F. *J. Phys. Chem. B* **1997**, *101*, 6799−6802.
(14) Ramakrishna, S.; Willig, F. *J. Phys. Chem. B* **2000**, *104*, 68−77.
(15) Tachibana, Y.; Moser, J. E.; Grätzel, M.; Klug, D. R.; Durrant, J. R. *J. Phys. Chem.* **1996**, *100*, 20056−20062.
(16) Ellingson, R. J.; Asbury, J. B.; Ferrere, S.; Ghosh, H. N.; Sprague, J. R.; Lian, T.; Nozik, A. J. *J. Phys. Chem. B* **1998**, *102*, 6455−6458.
(17) Martini, I.; Hodak, J. H.; Hartland, G. V. *J. Phys. Chem. B* **1998**, *102*, 9508−9517.
(18) Yan, S. G.; Hupp, J. T. *J. Phys. Chem.* **1996**, *100*, 6867−6870.
(19) Haque, S. A.; Tachibana, Y.; Klug, D. A.; Durrant, J. A. *J. Phys. Chem. B* **1998**, *102*, 1745−1749.
(20) Kelly, C. A.; Farzad, F.; Thompson, D. A.; Stipkala, J. M.; Meyer, G. J. *Langmuir* **1999**, *15*, 7047−7054.
(21) Kamat, P. V.; Bedja, I.; Hotchandani, S.; Patterson, L. K. *J. Phys. Chem.* **1996**, *100*, 4900−4908.
(22) Nasr, C.; Kamat, P. V.; Hotchandani, S. *J. Phys. Chem. B* **1998**, *102*, 10047−10056.
(23) Hilgendorff, M.; Sundström, V. *J. Phys. Chem. B* **1998**, *102*, 10505−10514.
(24) Yan, S. G.; Prieskorn, J. S.; Kim, Y.; Hupp, J. T. *J. Phys Chem. B* **2000**, in publication.
(25) Lu, H.; Prieskorn, J. N.; Hupp, J. T. *J. Am. Chem. Soc.* **1993**, *115*, 4927−4928.
(26) Martini, I.; Hodak, J. H.; Hartland, G. V. *J. Phys. Chem. B* **1998**, *102*, 607−614.
(27) Hasselman, G. M.; Meyer, G. J. *J. Phys. Chem. B* **1999**, *103*, 7671−7675.
(28) Tachibana, Y.; Haque, S. A.; Mercer, I. P.; Durrant, J. R.; Klug, D. A. *J. Phys. Chem. B* **2000**, *104*, 1198−1205.
(29) Ford, W. E.; Rodgers, M. A. J. *J. Phys. Chem.* **1994**, *98*, 3822−3831.
(30) Ford, W. E.; Wessels, J. M.; Rodgers, M. A. J. *Langmuir* **1996**, *12*, 3449−3453.
(31) Liu, D.; Fessenden, R. W.; Hug, G. L.; Kamat, P. V. *J. Phys. Chem. B* **1997**, *101*, 2583−2590.
(32) Mulvaney, P.; Grieser, F.; Meisel, D. *Langmuir* **1990**, *6*, 567−572.
(33) Nasr, C.; Hotchandani, S.; Kamat, P. V.; Das, S.; George Thomas, K.; George, M. V. *Langmuir* **1995**, *11*, 1777−1783.
(34) Dang, X.; Hupp, J. T. *J. Am. Chem. Soc.* **1999**, *121*, 8399−8400.
(35) *Lange's Handbook of Chemistry*, 13th ed.; McGraw-Hill: New York, 1985.
(36) Fussa-Rydel, O.; Zhang, H.; Hupp, J. T.; Leidner, C. R. *Inorg. Chem.* **1989**, *28*, 1533−1537.
(37) Kober, E. M.; Caspar, J. V.; Sullivan, B. P.; Meyer, T. J. *Inorg. Chem.* **1988**, *27*, 4587−4598.
(38) Juris, A.; Balzani, V.; Barigelletti, F.; Campagna, S.; Belser, P.; Von Zelewsky, A. *Coord. Chem. Rev.* **1988**, *84*, 85−277.

ligand) with either L or a monodentate ligand. In the case of the tris complexes, $Os(L)_2Cl_2$ was suspended in degassed 1:1 EtOH/H_2O with at least 4 times excess L. The reaction was heated to reflux for 8−12 h and allowed to cool. The brown solution was filtered to remove any unreacted starting material and placed under vacuum to remove EtOH. An aqueous solution of NH_4PF_6 was added, and the precipitated solid was isolated by filtration. Comparison of electrochemical values[39] and ^{1}H NMR were used to ensure identity of the isolated complexes followed by metathesis to the Cl^- salt. Typical yields were 70−80%.

For the bis-phenanthroline complexes, *cis*-$Os(L)_2Cl_2$ was suspended in degassed ethylene glycol with approximately 40 times excess 4-pyrrolidinopyridine (4pypy) or 1-methylimidazole (m-im) and heated to reflux for 4 h and allowed to cool. The brown solution was filtered to remove any unreacted starting material and aqueous KPF_6 was added. The precipitate was collected by filtration and rinsed with H_2O and ether. Mixtures of the monosubstituted and disubstituted product were separated by column chromatography on neutral alumina with acetonitrile:toluene mixtures as eluent. The disubstituted products, all of which are variants of known compounds, were characterized electrochemically and by high-resolution FAB mass spectrometry. Metathesis to the Cl^- salt was performed in the same manner as previously described. Typical yields varied from 60 to 80%. HR FAB-MS (*m*/*z*): $[Os(phen)_2(4pypy)_2]Cl_2$ $[M - Cl]^+$ calcd for $OsC_{42}H_{40}N_8Cl$, 883.2679; found, 883.2688. $[Os(4,7\text{-dimethylphen})_2(4pypy)_2]Cl_2$ $[M - Cl]^+$ calcd for $OsC_{46}H_{48}N_8Cl$, 939.3305; found, 939.3297. $[Os(3,4,7,8\text{-tetramethylphen})_2(4pypy)_2]Cl_2$ $[M - Cl]^+$ calcd for $OsC_{50}H_{56}N_8Cl$, 995.3931; found, 995.3927. $[Os(phen)_2(m\text{-im})_2]Cl_2$ $[M - Cl]^+$ calcd for $OsC_{32}H_{28}N_8Cl$, 751.1740; found, 751.1731. $[Os(4,7\text{-dimethylphen})_2(m\text{-im})_2]Cl_2$ $[M - Cl]^+$ calcd for $OsC_{36}H_{36}N_8Cl$, 807.2366, found, 807.2356. $[Os(3,4,7,8\text{-tetramethylphen})_2(m\text{-im})_2]Cl_2$ $[M - Cl]^+$ calcd for $OsC_{40}H_{44}N_8Cl$, 863.2992; found, 863.2985.

Sample Preparation. Dye solutions (15 μM) were prepared with the appropriate amount of SnO_2 to achieve quenching of 95% of the dye luminescence; this ensures that at least 95% of the dye molecules are bound to the semiconductor surface. The solutions were approximately pH 9 when diluted with pure water. For variable pH studies, 1 mM NaOH or 1 mM HCl was added during the preparation of the solutions along with appropriate amounts of NaCl so that the solution ionic strength (neglecting contributions from the charged tin oxide particles and counterions) was held constant at 1 mM.

Measurements. ^{1}H NMR spectra were obtained on a Varian-Gemini 300 MHz NMR spectrometer in either d_6-acetone or D_2O, depending on the counterion. UV−visible spectral measurements were performed with a HP 8452A diode array spectrophotometer. Electrochemical measurements were performed with an EG&G PAR 273 potentiostat using a conventional one-compartment, three-electrode cell. The working electrode was a glassy carbon electrode with a platinum wire as the counter electrode. A Ag/AgCl reference electrode was used with the results corrected to SCE[40] for comparison with literature values. Samples were dissolved in 0.1 M tetrabutylammonium hexafluorophosphate/acetonitrile solution. The cyclic voltammograms were collected at 100 mV/s. Luminescence studies were performed on an ISA Fluorolog-3 spectrofluorimeter by excitation at the absorption maximum in air saturated solutions. Low- and high-resolution FAB-MS were obtained on the ZAB-SE mass spectrometer and the 70-SE-4F mass spectrometer, respectively, at the Mass Spectrometry Laboratory, School of Chemical Sciences, University of Illinois. Transient absorbance spectra were obtained with a 10-Hz Nd:YAG laser system,[41] using the 532 nm second harmonic of the laser as the pump. The probe light was generated by a xenon flashlamp (EG&G Electro-optics FX-200) and detected by a photomultiplier tube (Hamamatsu R928). Traces measuring the bleach recovery at the MLCT maximum were time-resolved with a LeCroy 9384 oscilloscope and averaged by computer. Transient absorbance spectra were fit to a double exponential expression of the form: $\Delta A(t) = \Delta A_0[a \exp(-k_{1,app}t) + b \exp(-k_{2,app}t)] + \text{constant}$, with correction for the 8 ns laser pulse width and instrument response. The larger rate constant was used in analysis of the ET process with the smaller rate constant consistently equaling $\sim 10^5$ s^{-1}.

(39) Leidner, C. R.; Murray, R. V. *J. Am. Chem. Soc.* **1984**, *106*, 1606.
(40) Bard, A. J.; Faulkner, R. *Electrochemical Methods: Fundamentals and Applications*; Wiley-Interscience: New York, 1980.
(41) Greenfield, S. R.; Svec, W. A.; Gosztola, D.; Wasielewski, M. R. *J. Am. Chem. Soc.* **1996**, *118*, 6767−6777.

Results and Discussion

From preliminary studies involving ruthenium tris(polypyridyl) complexes electrostatically bound to colloidal SnO_2,[34] the following mechanistic sequence was inferred:

$$Ru^{II}L_3^{2+} + h\nu \rightarrow RuL_3^{2*+} \quad \text{MLCT excitation} \qquad (3)$$

$$RuL_3^{2*+} + SnO_2 \rightarrow Ru^{III}L_3^{3+} + SnO_2(e^-_{cb}) \quad \text{electron injection} \qquad (4)$$

$$Ru^{III}L_3^{3+} + SnO_2(e^-_{cb}) \rightarrow Ru^{II}L_3^{2+} + SnO_2 \quad \text{back electron transfer} \qquad (5)$$

The key features of the mechanism are: (a) the transfer of electrons directly to and from the semiconductor's conduction band (as opposed to trap states) and (b) over the limited range of driving forces examined (−1.9 to −2.3 eV), the occurrence of Marcus-type inverted reactivity—a finding that appeared reasonable, given an estimated reorganization energy of ~0.5 eV.[42]

To expand upon these studies, a series of osmium(II) tris(polypyridine) and bis(polypyridine) complexes was evaluated. Like their ruthenium congeners, these species feature low-spin d^6 electronic configurations and undergo reversible one-electron oxidation (nonbonding electron loss) by a process that is believed to involve significant reorganization of only the solvent. Osmium complexes have been used previously as sensitizers on TiO_2 with the primary differences between the ruthenium and osmium derivatives being less positive metal(III/II) potentials and increased extinction at longer wavelengths for the latter.[43−45] The combination of osmium and ruthenium sensitizers creates an extended set of ET reactants of similar structure but of widely varying redox potential. Indeed, as indicated in Table 1, the potentials for the available couples and, therefore, the driving forces for back ET span a range of greater than 1 V. Using these osmium complexes, the details of the back ET mechanism were elucidated by studying four important properties of the reaction kinetics: the incident laser power dependence, the dye-based driving force dependence, the solution pH dependence, and the temperature dependence.

A. Excitation Pulse Power Dependence and Reaction Order of the Back Electron-Transfer Process. The reaction scheme embodied in eqs 3−5 yields testable predictions concerning reaction order. Specifically, eq 5 promises back-reaction kinetic behavior that is first-order in Ru(III) (or Os(III)) and simultaneously first-order with respect to electron concentration. Recognizing that for intrinsic or poorly doped semiconductors, the only significant source of conduction band electrons is dye injection (eq 3), the back reaction will not only be equal order in electrons and oxidized dye, but will also draw upon equal populations of the two reactants.[46] This implies, of

(42) Clark, W. D. K.; Sutin, N. *J. Am. Chem. Soc.* **1977**, *99*, 4676−4682.
(43) Heimer, T. A.; Bignozzi, C. A.; Meyer, G. J. *J. Phys. Chem.* **1993**, *97*, 11987−11994.
(44) Alebbi, M.; Bignozzi, C. A.; Heimer, T. A.; Hasselmann, G. M.; Meyer, G. J. *J. Phys. Chem. B* **1998**, *102*, 7577−7581.
(45) Sauve, G.; Cass, M. E.; Doig, S. J.; Lauermann, I.; Pomykal, K.; Lewis, N. S. *J. Phys. Chem. B* **2000**, *104*, 3488−3491.
(46) Molar concentrations, on the other hand, are not anticipated to be equal because the electron and oxidized dye populations are confined to different regions of space (i.e., inside vs outside the semiconductor particles) and generally different volumes.

Table 1. Electrochemical Data, Driving Force Information, and Electron Transfer Values for All Ru and Os Sensitizers

compound	E_f (V, vs SCE)	ΔG_{bET} (eV) (pH = 9)	$k_{ET}\beta \times 10^{13}$ ($cm^3\ s^{-1}$)	ΔH^* (kJ/mol)
$Ru(5\text{-}Cl\text{-}phen)_3^{2+}$	1.39[a]	−2.27	0.76	18.2
$Ru(phen)_3^{2+}$	1.27[a]	−2.15	1.70	15.4
$Ru(bpy)_3^{2+}$	1.29[a]	−2.17	1.74	14.5
$Ru(5\text{-}CH_3\text{-}phen)_3^{2+}$	1.26[a]	−2.14	1.82	13.0
$Ru(5,6\text{-}CH_3\text{-}phen)_3^{2+}$	1.23[a]	−2.11	1.66	9.50
$Ru(4,7\text{-}CH_3\text{-}phen)_3^{2+}$	1.12[a]	−2.00	2.95	6.70
$Ru(3,4,7,8\text{-}CH_3\text{-}phen)_3^{2+}$	1.05[a]	−1.93	6.76	4.40
$Os(5\text{-}Cl\text{-}phen)_3^{2+}$	0.90[b]	−1.78	5.13	4.50
$Os(phen)_3^{2+}$	0.80[c]	−1.68	10.2	3.20
$Os(4\text{-}CH_3\text{-}phen)_3^{2+}$	0.79[c]	−1.67	11.5	3.50
$Os(4,7\text{-}CH_3\text{-}phen)_3^{2+}$	0.62[c]	−1.50	13.8	3.00
$Os(3,4,7,8\text{-}CH_3\text{-}phen)_3^{2+}$	0.57[b]	−1.45	14.5	2.90
$Os(phen)_2(4pypy)_2^{2+}$	0.52[c]	−1.40	16.6	3.20
$Os(phen)_2(m\text{-}im)_2^{2+}$	0.46[c]	−1.34	12.9	3.20
$Os(4,7\text{-}CH_3\text{-}phen)_2(4pypy)_2^{2+}$	0.41[c]	−1.29	16.2	3.40
$Os(4,7\text{-}CH_3\text{-}phen)_2(m\text{-}im)_2^{2+}$	0.38[c]	−1.26	12.3	12.0
$Os(3,4,7,8\text{-}CH_3\text{-}phen)_2(4pypy)_2^{2+}$	0.35[c]	−1.23	12.9	6.40
$Os(3,4,7,8\text{-}CH_3\text{-}phen)_2(m\text{-}im)_2^{2+}$	0.31[c]	−1.19	10.7	10.90

[a] Reference 38. [b] Reference 39. [c] Experimentally measured and corrected from Ag/AgCl to SCE.

Scheme 2

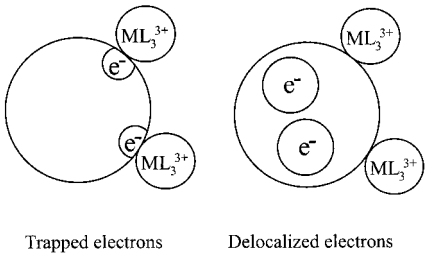

course, that if we know the population of oxidized dye molecules we necessarily know the population of electrons—an otherwise somewhat elusive quantity. In any case, with overall second-order kinetics, the lifetime (τ_1) of the back reaction is expected to decrease and the apparent rate constant ($k_{1,app} = 1/\tau_1$) is expected to increase, if the initial concentrations of oxidized dye and injected electrons increase. The initial concentrations can be readily manipulated by altering the laser excitation pulse intensity.

An alternative reaction scenario is one in which each electron is very rapidly trapped at a site sufficiently proximal to the parent dye that the electron and oxidized dye behave as a geminate pair. The reaction rate is thus first-order in the pair, rather than first-order in each component; see Scheme 2. Under these conditions the back-reaction lifetime will be unaffected by changes in laser excitation power. Behavior of this kind has been reported in at least a few instances for reactions involving transition-metal complexes strongly bound to titanium dioxide.[7,47,48]

Figure 1 shows a representative power-dependence or reaction-order plot for the sensitizer, $Os(phen)_3^{2+}$. The plot is formulated as $k_{1,app}$ versus η_e, the number of injected conduction band electrons per unit volume of tin oxide (bottom axis), and versus η_{ep}, the number of injected conduction band electrons per particle (top axis), where we have assumed an average single-particle volume of 1.8×10^{-18} cm^3. The required η_e values were obtained by first determining the concentration of injected electrons for each sample ($(\Delta A/A)[M^{II}]$) and dividing by the molarity of SnO_2 particles (determined from concentration and estimated size and density) and the volume of the SnO_2 particles. The figure shows that multiple electrons are injected per particle and that the apparent rate constant is a linear, or approximately linear, function of the electron concentration. The results are consistent, therefore, with the overall second-order reaction scheme suggested by eqs 3−5.

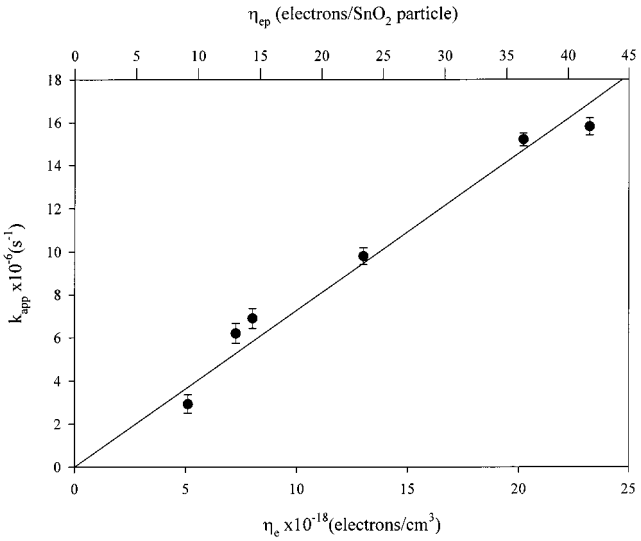

Figure 1. Plot of apparent rate constant for back ET to $Os(phen)_3^{3+}$ versus η_e, the number of injected electrons per unit volume of SnO_2 (bottom axis) and η_{ep}, the number of injected electrons per SnO_2 particle (top axis). The line is a best fit line constrained to pass through the origin.

Given the second-order behavior, reactivity comparisons for various complexes are meaningful only if $k_{1,app}$ values are obtained at the same initial electron concentration or, better yet, if comparisons are made on the basis of second-order rate constants, k_{ET}. Following Lewis and co-workers,[49,50] the back-

(47) Heimer, T. A.; Heilweil, E. J.; Bignozzi, C. A.; Meyer, G. J. *J. Phys. Chem. A* **2000**, *104*, 4256−4262.

(48) A third scenario is one involving electron trapping, but with significant hopping among trap states, rather than immobilization. If the hopping is sufficiently spatially extensive that the injected electron is not compelled to return to the parent dye but can instead recombine with any available oxidized dye molecule and if the hopping itself is kinetically limiting, the back-reaction lifetime is expected to shorten as the laser excitation power increases. This behavior is similar, therefore, to that expected for conduction-band-based back ET (eq 5). In contrast to eq 5, however, the reaction rate in the third scenario is expected to be insensitive to changes in the overall back-reaction driving force,[27,28] and can therefore be ruled out here ($k_{1,app}$ process; see section B). Conceivably, however, such behavior is important at longer times ($k_{2,app}$ processes).

(49) Royea, W. J.; Fajardo, A. M.; Lewis, N. S. *J. Phys. Chem. B* **1997**, *101*, 11152−11159.

(50) Lewis, N. S. *Annu. Rev. Phys. Chem* **1991**, *42*, 543−580.

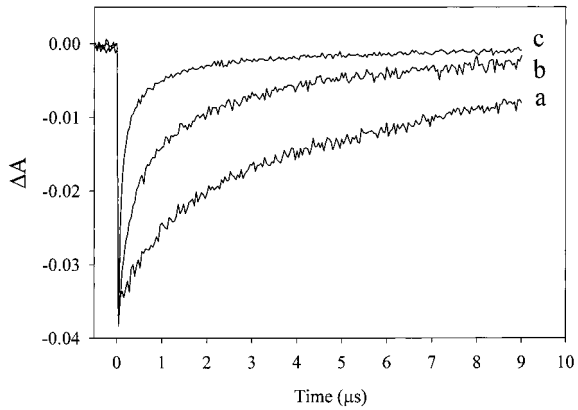

Figure 2. Transient absorbance data obtained at the respective MLCT maximum (following excitation at 532 nm) for aqueous SnO_2 colloid sensitized with: (a) $Ru(5\text{-Cl-phen})_3^{2+}$, (b) $Ru(4,7\text{-}CH_3\text{-phen})_3^{2+}$, and (c) $Os(phen)_3^{2+}$.

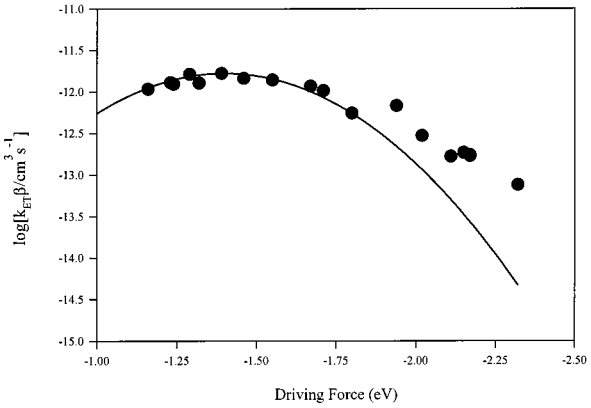

Figure 3. Plot of $\log(k_{ET}\beta)$ versus free-energy driving force. Solid line is the classical rate vs driving force relationship predicted by eq 1. Departure of the experimental data from the calculated classical curve in the inverted region is interpreted as nonclassical (quantum mechanical) rate behavior.

reaction rate can be written as:

$$\text{rate} = (1/\tau_1)\Gamma(M^{III}L_3^{3+}) = k_{1,app}\Gamma(M^{III}L_3^{3+}) = k_{ET}\beta\eta_e\Gamma(M^{III}L_3^{3+}) \quad (6)$$

where $\Gamma(M^{III}L_3^{3+})$ is the concentration of oxidized dye on the semiconductor surface (mol cm^{-2}), and β is the electronic coupling attenuation factor (value unknown, but typically estimated as $0.4 < \beta < 1.5$ $Å^{-1}$ for ET in molecular systems). In this formulation, the units of k_{ET} are cm^4 s^{-1}, as expected for a second-order interfacial process.

Because the value of β is unknown, we have chosen to report the composite quantity $k_{ET}\beta$ obtained from the slopes of best fit lines of plots of $k_{1,app}$ versus η_e, constrained to pass through the origin. For the system in Figure 1, the value of $k_{ET}\beta$ is 1.0×10^{-12} cm^3 s^{-1}.

B. Driving Force Dependence of the Back Electron-Transfer Rate. Figure 2 shows representative visible-region transient absorbance recovery traces for three sensitizers—$Ru(5\text{-Cl-phen})_3^{2+}$, $Ru(4,7\text{-}CH_3\text{-phen})_3^{2+}$, and $Os(phen)_3^{2+}$—electrostatically bound to SnO_2. While uncorrected for concentration and absorptivity differences, the traces are strongly suggestive of differing second-order reactivity. The suggestion is borne out by Table 1 which lists the $k_{ET}\beta$ values obtained for each of the 18 reactants. Note that the reported values are for ambient temperature conditions in aqueous solution at pH = 9.

Figure 3 shows that $k_{ET}\beta$ varies systematically with the thermodynamic driving force, where the driving force is approximated as the difference between the tin oxide conduction band-edge potential (−0.88 V vs SCE at pH 9) and the ground-state metal (III/II) formal potential. Furthermore, the behavior observed is in good qualitative agreement with the behavior expected from Marcus theory:[2] $\log(k_{ET}\beta)$ initially increases with increasing driving force ($\Delta G = -1.3$ to -1.4 eV; the increase is more persuasively indicated in variable-temperature kinetic studies described below) but then decreases in a more or less parabolic fashion as the driving force is further amplified ($\Delta G = -1.5$ to -2.3 eV). To the best of our knowledge, this is the first experimental example of interfacial back ET reactivity that spans the normal and inverted regions.[51]

The observation of both kinetic regimes within a single family of reactions permits the total reorganization energy (λ) to be determined with some confidence. Recall (eq 2) that ET rate constants reach their maximum value when $-\Delta G = \lambda$. On that basis λ is ~1.4 eV—a surprisingly large value. For comparison, Brown and Sutin[52] report a kinetically derived reorganization energy of ~0.8 eV for RuL_3^{3+}/RuL_3^{2+} self-exchange in homogeneous solution—a quantity that should significantly exceed the interfacial reorganization energy because of the bimolecular nature of the former.[53]

From Brown and Sutin's work and from X-ray crystallographic studies of a related redox pair, $Fe(phen)_3^{3+}/Fe(phen)_3^{2+}$, that indicates no detectable difference in $M^{III}-N$ vs $M^{II}-N$ bond lengths,[54] the vibrational component of the reorganization energy for tris(polypyridyl)−ruthenium(III/II) and −osmium(III/II) redox reactions has generally been assumed to be close to zero. Standard interfacial ET theory[2] yields an estimated solvent reorganizational contribution for eq 5 of just 0.3−0.6 eV, [55,56] leaving roughly 1 eV of reorganization unaccounted for. One possibility is that significant reorganizational demands also exist on the semiconductor side of the interface—and, indeed,

(51) Studies on band gap excitation of MoS_2 with subsequent interfacial electron transfer (forward ET) to adsorbed electron acceptors have provided evidence for both normal and inverted region behavior. See: Parsapour, F.; Kelley, D. F.; Craft, S.; and Wilcoxon, J. P. *J. Chem. Phys.***1996**, *104*, 4978−4987.

(52) Brown, G. M.; Sutin, N. *J. Am. Chem. Soc.* **1979**, *101*, 883−892.

(53) One possible alternative explanation is that despite the reaction-order findings, back ET occurs from deep traps. The true driving force would then be much less than the driving force obtained from the difference in energy between the conduction band-edge and the formal oxidation potential of the dye. The energy at the maximum in the $k_{ET}\beta$ vs $-\Delta G$ plot, corresponding to λ, would then be much less than 1.4 eV. Direct measurement of the overall back-reaction thermodynamics via time-resolved photoacoustic spectroscopy show, however, that the driving forces are not smaller than expected from band-edge/formal potential differences (Leytner, S. and Hupp, J. T., unpublished studies).

(54) Brunschwig, B. S.; Creutz, C.; MaCartney, D. H.; Sham, T. K.; Sutin, N. *Faraday Discuss. Chem. Soc.* **1982**, *74*, 113−127.

(55) The solvent reorganization energy (λ_s) was calculated from:

$$\lambda_s = \frac{(\Delta e)^2}{8\pi\epsilon_0}\left(\frac{2}{d} - \frac{1}{2r}\right)\left(\frac{1}{n^2} - \frac{1}{\epsilon}\right)$$

where d is the diameter of the molecule, r is the mean ET distance, n is the refractive index of the solvent (1.34 for H_2O at 25 °C), and ϵ is the static dielectric constant of the solvent (78.4 for H_2O at 25 °C). Assuming d to be 14 Å[54] and r being 7 Å, the distance from the metal center to the surface, $\lambda_s \approx 0.3$ eV. If the $1/2r$ term is omitted (due to image charge screening as suggested by Hush (*Trans. Faraday Soc.* **1961**, *57*, 557)), the value calculated for λ_s is ~0.6 eV.

(56) An experimental study by Hupp and Zhang (*J. Phys. Chem.* **1995**, *93*, 853−855) of interfacial ET kinetics at the highly oriented pyrolitic-graphite/water interface, based in part on even earlier work by Kneten and McCreery (*Anal. Chem.* **1992**, *64*, 2518−2524), implies a solvent reorganization energy of just 0.3−0.4 eV for the $Fe(phen)_3^{3+/2+}$ couple.

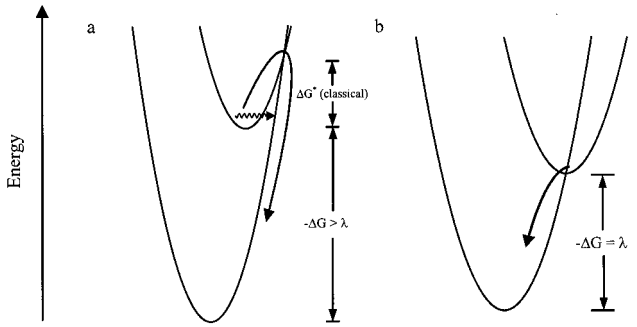

Figure 4. (a) Schematic representation of back-electron energetics in the inverted region, showing fully activated (classical barrier crossing) and completely unactivated (quantum mechanical barrier tunneling) pathways. (b) Schematic representation of barrierless ET energetics achieved when $-\Delta G_{ET} = \lambda$.

resonance Raman studies of ET between $Fe(CN)_6^{4-}$ and titanium dioxide offer one example of such an effect (albeit, with contributions amounting to much less than 1 eV).[57] The $Fe(CN)_6^{4-}/TiO_2$ system, however, differs importantly from the current system in that it involves strong chemical interactions and probable electron trap-state participation. It seems unlikely to us that weakly adsorbed dyes and delocalized conduction band electrons could impose similar reorganizational demands upon the tin oxide lattice.

Returning to Figure 3, a more quantitative treatment—a comparison to the classical rate versus driving force profile predicted by eq 1, based on $\lambda = 1.4$ eV—shows that measured rates exceed calculated rates in the inverted region, and increasingly so, as the driving force increases. The most probable cause is the existence of high-frequency reorganizational components, that is, components that behave nonclassically and are incorrectly treated, therefore, by classical models (Figure 4a). If, for the sake of illustration, we assume that the back-reaction reorganization energy can be partitioned into just two components—a single high-frequency, nonclassical component, λ_{nc}, and a collective low-frequency, classical component, λ_c—and if we further assume a nonclassical vibrational frequency of 1600 cm^{-1} (appropriate, for example, to a hypothetical back-bonding-induced displacement of bipyridine ring breathing modes), the experimental driving force plot can be reasonably well-reproduced with $\lambda_{nc} = 0.5$ eV and $\lambda_c = 0.9$ eV.[58] If the nonclassical component is instead arbitrarily assigned a frequency of 800 cm^{-1}, the experimental behavior is best replicated with $\lambda_{nc} = 1.0$ eV and $\lambda_c = 0.4$ eV.

C. Barrierless Reactions and Electronic Coupling Effects. Regardless of the origin of the large reorganization energy, the availability of data obtained under conditions of equally large driving force permits the kinetics of back ET to be examined under barrierless conditions (Figure 4b).[59,60] This, in turn, permits metal-complex/semiconductor electronic interactions to be investigated. Briefly, reactions occurring at the top of the driving force plot in Figure 3 (i.e., at $\Delta G \approx -\lambda$) are unconstrained by vibrational or solvational reorganization and are kinetically limited instead only by dynamical effects. These, in turn, are governed, under nonadiabatic conditions, by the initial-state/final-state electronic coupling energy, H_{ab}. Following Royea et al.,[49] who assumed conventional radiationless-decay type kinetics, the maximum rate constant (barrierless rate constant) for a weakly nonadiabatic ET at a semiconductor surface with a random distribution of redox acceptors can be described by the following expression:

$$k_{ET,max} = (4\pi^2/h)[(4\pi kT\lambda)^{-1/2}](H_{ab}{}^2)(\beta^{-1})[(l_{sc}/(d_{sc}{}^{2/3}(6/\pi)^{1/3})] \quad (7)$$

In the equation, l_{sc} is the effective coupling length of the redox acceptor wave function into the semiconductor, d_{sc} is the atomic density of the semiconductor, h is Planck's constant, and k is the Boltzmann constant. Unfortunately, quantitative information about β and l_{sc} is lacking. Nevertheless, if we assume, for the moment, that β equals 1 $Å^{-1}$ and l_{sc} equals 1 Å and apply eq 7 to the back ET reaction involving $Os(phen)_2(4pypy)_2^{3+}$ ($\Delta G = -1.40$ eV $\approx -\lambda$), we obtain an H_{ab} value of approximately 30 cm^{-1}. The apparent coupling constant is smaller than the frequencies of potentially Franck—Condon active metal—ligand modes, semiconductor phonon modes, and solvent (water) vibrational modes, as well as the frequency of solvent longitudinal relaxation. This strongly suggests that: (a) the quantity derived from eq 7 indeed does correspond, at least approximately, to the electronic coupling energy, and (b) the assumption of weakly nonadiabatic reactivity is correct. Similar analyses of back ET to $Os(3,4,7,8\text{-}CH_3\text{-}phen)_3^{3+}$ ($\Delta G = -1.45$ eV) and $Os(4,7\text{-}CH_3\text{-}phen)_2(4pypy)_2^{3+}$ ($\Delta G = -1.29$ eV) yield estimated H_{ab} values of 15 and 30 cm^{-1}, respectively. The approximate constancy of H_{ab} for the three systems is notable, especially in view of the ET distance variations that conceivably could be induced by the introduction of multiple methyl substituents (i.e., potential spacers). The finding is consistent, however, with the comparatively smooth variation of $\log(k_{ET}\beta)$ with reaction driving force in Figure 3. Indeed, substantive deviations traceable to ligand structural effects appear to be absent from the rate correlation.

D. pH Dependence of the Back Electron-Transfer Rate. In principle, pH variations provide another means of altering the back-reaction driving force. As illustrated in Figure 5, adjustment of pH leads to a Nernstian shift (−59 mV/pH unit) in the position of the conduction band-edge of SnO_2[61,62] and, therefore, the free energy of the electron. The effects of pH-induced changes in driving force are shown in Figure 6 for back ET to $Os(5\text{-}Cl\text{-}phen)_3^{3+}$, an inverted region system, and $Os(3,4,7,8\text{-}CH_3\text{-}phen)_2(m\text{-}im)_2^{3+}$, a normal region system (also see Supporting Information). Due to constraints associated with the need to maintain a negative colloidal particle surface charge

(57) Blackbourn, R. L.; Johnson, C. S.; Hupp, J. T. *J. Am. Chem. Soc.* **1991**, *113*, 1060−1062.

(58) Nonclassical or quantum mechanical rate constants were calculated from:

$$k = \frac{H_{ab}{}^2}{\hbar}\left(\frac{\pi}{\lambda_s RT}\right)^{1/2}\exp\left[-\sum_j S_j \coth\left(\frac{\hbar\omega_j}{2kT}\right)\right]\times\prod_j\sum_{m_j=-\infty}^{+\infty}\exp\left(\frac{m_j\hbar\omega_j}{2kT}\right)I_{m_j}\left\{S_j\,\mathrm{csch}\left(\frac{\hbar\omega_j}{2kT}\right)\right\}\times\exp\left[\frac{(\Delta E+\sum_j m_j\hbar\omega_j+\lambda_s)^2}{4\lambda_s RT}\right]$$

where S equals $\Delta^2/2$ and Δ is the unitless normal coordinate displacement for each Franck—Condon active vibrational mode, ω is 2π times the normal mode vibrational frequency, m is the change in vibrational quantum number, I_m is a modified Bessel function of order m, and ΔE is the difference in energy between the initial state and the final state. For a particularly clear discussion, see Brunschwig, B. S.; Sutin, N. *Comments Inorg. Chem.* **1987**, *6*, 209−235.

(59) Fajardo, A. M.; Lewis, N. S. *J. Phys. Chem. B* **1997**, *101*, 11136−11151.

(60) Pomykal, K. E.; Fajardo, A. M.; Lewis, N. S. *J. Phys. Chem* **1996**, *100*, 3652−3664.

(61) Watanabe, T.; Fujishima, A.; Tatsuoki, O.; Honda, K. *Bull. Chem. Soc. Jpn.* **1976**, *49*, 8−11.

(62) Bolts, J. M.; Wrighton, M. S. *J. Phys. Chem.* **1976**, *80*, 2641−2645.

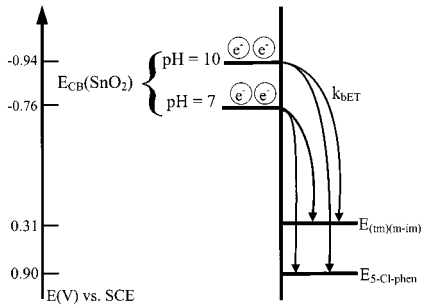

Figure 5. Schematic representation of the pH dependence of the conduction band-edge energy of SnO_2 and the predicted pH dependence of the driving force for back ET to Os(5-Cl-phen)$_3^{3+}$ and Os(3,4,7,8-CH_3-phen)$_2$(m-im)$_2^{3+}$.

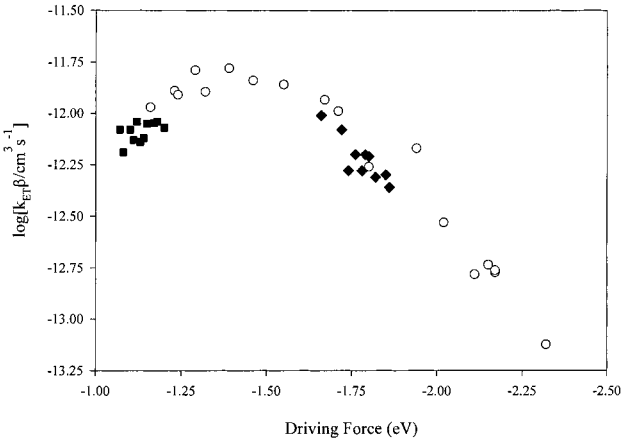

Figure 6. Plot of log($k_{ET}\beta$) vs free-energy driving force at several pHs between 7 and 10 for Os(5-Cl-phen)$_3^{3+}$ (♦) and Os(3,4,7,8-CH_3-phen)$_2$(m-im)$_2^{3+}$ (■). Shown for comparison (○) are data obtained at pH = 9 for all reactants.

and to maintain a low ionic strength, the pH was varied only between 7 and 10. Even over this range, however, it is clear in both instances that increasing the pH has an effect—slightly accelerating back ET to Os(3,4,7,8-CH_3-phen)$_2$(m-im)$_2^{3+}$, and more substantially decelerating back ET to Os(5-Cl-phen)$_3^{3+}$. Furthermore, as shown in Figure 6, the pH-induced driving force effects can be more or less quantitatively mapped onto the broader formal potential-based rate vs driving force correlation. The findings are clearly consistent with overall kinetic control via reaction 5 (or equivalent reactions involving Os(III) species).

The pH-sensitive rate behavior found here can be contrasted with the pH independence observed for back ET to related reactants covalently bound to TiO_2; there a somewhat more complicated trap-based mechanism for back ET has been suggested.[18,24,63] It remains to be determined whether covalent attachment to SnO_2 similarly alters the pH sensitivity.

E. Temperature Dependence of the Back Electron-Transfer Rate. Variable-temperature kinetics studies were undertaken to gain further insight into the nature of the reorganizational processes necessarily accompanying back ET. Of particular interest to us was the magnitude of the apparent activation enthalpy, ΔH^*. A phenomenological formulation of the activation problem in terms of Royea and Lewis' interfacial rate expressions is the following:

$$k_{1,\mathrm{app}} = \eta_e (4\pi^2 H_{ab}{}^2/h)(4\pi\lambda_s RT)^{-1/2} [(l_{sc}/(d_{sc}{}^{2/3}(6/\pi)^{1/3}))] \exp[\Delta S^*/R] \exp[-\Delta H^*/RT] \quad (8)$$

(63) Yan, S. G.; Hupp, J. T. *Proc. Electrochem. Soc.* **1996**, *96*, 53−64.

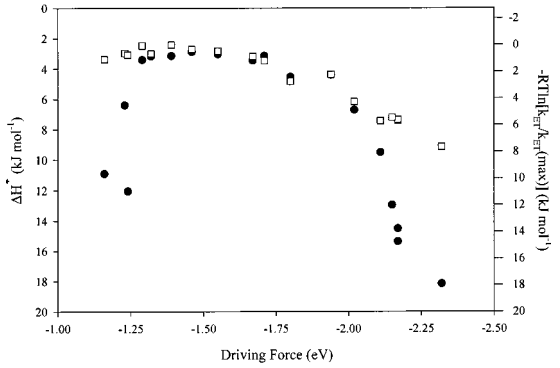

Figure 7. Plot of measured activation enthalpy (●) and $-RT\ln[k_{ET}/k_{ET}(\mathrm{max})]$ (□), (Note that $-RT\ln[k_{ET}/k_{ET}(\mathrm{max})]$ is functionally equivalent to ΔG^*, assuming constant pre-factors in eq 1), for back ET versus free-energy driving force.

Provided that η_e is held constant (or equivalently, ΔA(initial) in a transient absorbance experiment is held constant) as the temperature is varied, ΔH^* for back ET can be obtained from a plot of $\ln(k_{1,\mathrm{app}}T^{1/2})$ vs $1/T$.[64]

We examined the back ET kinetics for each reactant over a temperature range of 20 to 60 °C; representative Arrhenius-like plots are included as Supporting Information, with activation enthalpy values listed for all reactions in Table 1. Figure 7—a plot of activation enthalpy versus free-energy driving force—summarizes the findings. As shown in the plot, back ET is thermally activated in both the normal and inverted kinetic regimes, but nearly activationless for reactions occurring at or near the maximum in the rate versus driving force plot in Figure 3. (We tentatively attribute the residual activation enthalpy for the fastest reactions (~2 kJ mol^{-1}) to neglect of a weakly temperature-dependent variable governing some other aspect of the kinetics, rather than to a true barrier-related activation effect.)

The existence of activated rate behavior in the inverted kinetic regime is unusual[65,66] but is qualitatively consistent with the idea that λ is a largely classical quantity (see section B). In the simplest case (fully classical behavior, with constant electronic coupling, and with $\Delta G^* = \Delta H^*$), variations in k_{ET} would be fully accounted for by variations in $\exp[-\Delta H^*/RT]$. Curiously, in the inverted region, activation enthalpy effects actually exceed the corresponding rate attenuation effects. For example, varying the back-reaction driving force from −1.8 to −2.3 eV leads experimentally to: (1) an increase in activation enthalpy from 4.5 to 18 kJ mol^{-1}, (2) a predicted 250-fold decrease in k_{ET}, but (3) an observed k_{ET} decrease of only 7-fold. The disparities are illustrated graphically in Figure 7 where, in addition to ΔH*, an appropriately normalized rate parameter, $-RT\ln[k_{ET}/k_{ET}(\mathrm{max})]$, has been plotted versus the back-reaction free-energy driving force.

One possible explanation for the rate/activation-enthalpy mismatch is that compensating entropic effects exist. For this to be true, ΔS^* would need to vary substantially with the overall free-energy driving force. Available classical treatments, in fact, make precisely this prediction when a significant entropic driving force (ΔS) exists. According to Sutin and Marcus:[3]

$$\Delta S^* = 0.5\Delta S + (\Delta G)(\Delta S)/2\lambda \quad (9)$$

The value of ΔS for the back ET process studied here is unknown, but values between roughly −200 and +200 J deg^{-1}

(64) Sutin, N. *Acc. Chem.* **1982**, *15*, 275−282.
(65) Wiedenfeld, D.; Bachrach, M.; McCleskey, T. M.; Hill, M. G.; Gray, H. B.; Winkler, J. R. *J. Phys. Chem. B* **1997**, *101*, 8823−8826.
(66) Moser, J. E.; Grätzel, M. *Chem. Phys.* **1993**, *176*, 493−500.

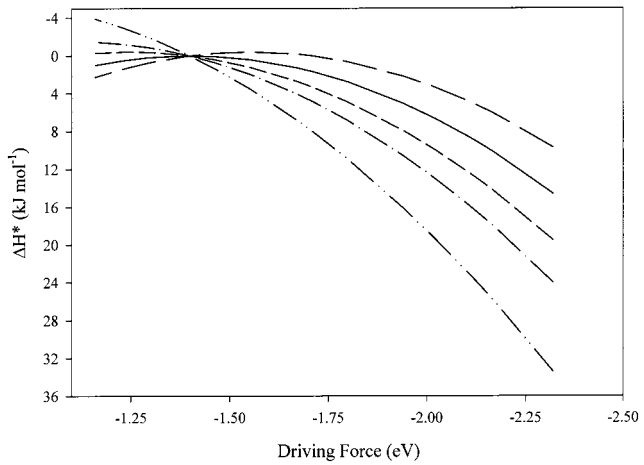

Figure 8. Calculated classical activation enthalpies as a function of driving force when $\lambda = 1.4$ eV (135 kJ mol^{-1}) and $\Delta S = +50$ J deg^{-1} mol^{-1} (— —), 0 J deg^{-1} mol^{-1} (—), -50 J deg^{-1} mol^{-1}(- - - -), -96 J deg^{-1} mol^{-1} (—·—), and -192 J deg^{-1} mol^{-1} (—··—).

mol^{-1} are typically seen for one-electron transfer reactions in water. Figure 8 shows representative calculated (hypothetical) classical activation enthalpy curves for back ET based on a range of ΔS values and a fixed reorganization energy of 1.4 eV (135 kJ mol^{-1}). The values were calculated from eqs 2 and 9, and the relationship: $\Delta H^* = \Delta G^* + T\Delta S^*$. From the figure, the enthalpy curve departs from the classical rate curve whenever ΔS is nonzero. When ΔS is negative, the departure occurs in a way that agrees qualitatively with experiment.[67]

The available evidence indicates, however, that back ET from tin oxide to the adsorbed polypyridyl Ru(III) or Os(III) complexes is a partially *non*classical kinetic process (see Figure 3 and section B, above). The classical activation-enthalpy modeling in Figure 7, therefore, is incomplete. To account simultaneously for nonclassical effects and for possible entropic driving force effects in modeling the back ET process and its temperature dependence, the following protocol was used: (a) Values for k_{ET} were calculated nonclassically at various driving forces and temperatures. (b) Entropic driving force effects were introduced into the calculation by allowing the driving force corresponding to any specific reaction to vary as a function of temperature ($\Delta S = -\partial\Delta G/\partial T$). (c) Phenomenological activation enthalpies were calculated by plotting $\ln[k_{ET}(\text{calc})T^{1/2}]$ vs $1/T$. Fair agreement with experiment, particularly in the inverted region, was obtained by assuming $\Delta S = -96$ J deg^{-1} mol^{-1} (-1 meV deg^{-1} mol^{-1}). For example, assuming an 800 cm^{-1} vibrational frequency, the activation enthalpy for the back ET to $Ru(phen)_3^{3+}$, experimentally determined to be 15.4 kJ mol^{-1}, was calculated to be 6 kJ mol^{-1} assuming an entropy driving force, but only 2.2 kJ mol^{-1} assuming $\Delta S = 0$. By increasing the entropic driving force effects by assuming $\Delta S = -192$ J deg^{-1} mol^{-1} (-2 meV deg^{-1} mol^{-1}), the agreement with experiment improved as an activation enthalpy of 10 kJ mol^{-1} was calculated.[68] We conclude that modest entropic driving forces likely exist for the back ET reactions and that the reactions involve both classical and high-frequency nuclear reorganization.

Conclusions

Electrostatic attachment of ruthenium and osmium tris-(polypyidyl) and bis(polypyridyl) complexes on colloidal SnO_2 particles has been used to investigate interfacial ET (back transfer) following dye injection. For the systems examined, electrostatic binding represents a weak enough perturbation that surface trapping of electrons is avoided, with electrons being transferred directly from the nanoparticle conduction band to the attached complexes. By manipulating the chemical structure and, therefore, the metal (III/II) potential of the attached complex, back ET driving force variations of greater than 1 eV were attained. These variations were sufficient to permit observation of Marcus normal region (low driving force), barrierless (intermediate driving force), and inverted (high driving force) kinetic behavior. The kinetics of back ET also proved amenable to modulation via pH-induced changes in the energy of the SnO_2 conduction band-edge and, therefore, the free-energy driving force. A semiquantitative interpretation of the barrierless rate behavior yielded an estimate of $\sim$15$-$30 cm^{-1} for the initial-state/final-state electronic coupling energy, H_{ab}—a value consistent with a moderately nonadiabatic back ET mechanism. From the observed maximum in a plot of log $k_{ET}\beta$ versus free-energy driving force, the reorganization energy for back ET is estimated to be 1.4 eV—a value significantly larger than expected based on prior work. Together with the results from variable-temperature kinetic meausrements, a more detailed analysis of the driving force effects points to the involvement of high-frequency modes (nonclassical modes) in the back ET process. The available data also suggest a significant entropic force for back ET exists.

In view of the rather striking differences in kinetic behavior for ET from SnO_2 to electrostatically attached compounds versus ET from TiO_2 to covalently attached compounds (a much stronger particle surface perturbation),[18,24,63] the question arises as to whether the differences reflect the method of attachment or rather the chemical composition of the semiconductor. The answer potentially has implications in terms of the design of new dye-based solar cells and the optimization of existing cells. We are currently investigating this interesting topic and hope to report the result in a future publication.

Acknowledgment. We thank Professor Michael Wasielewski for access to transient absorbance instrumentation and Xiaojun Dang, Ryan Hayes, and Dr. Svetlana Leytner for helpful discussions. We thank the Office of Naval Research for financial support.

Supporting Information Available: Changes in the back ET rate constant as a function of pH and modified Arrhenius plots (PDF). This material is available free of charge via the Internet at http://pubs.acs.org.

JA0024744

(67) Note that eq 9 and related equations predict, in the presence of a finite thermodynamic reaction entropy, a displacement of the maximum in the activation enthalpy curve with respect to the ΔG^* curve (or $\ln k_{ET}\beta$ curve); see Figure 8. The predicted degree of displacement is $T\Delta S$. It is difficult to determine from the data in Figure 7 whether such a displacement occurs experimentally. As pointed out by Marcus and Sutin (*Inorg. Chem.* **1975**, *14*, 213$-$216), eq 9 also predicts the existence of negative classical activation enthalpies at the top of the ΔH^* vs ΔG curve, whenever $\Delta S \neq 0$; see Figure 8. An experimental example of this unusual behavior has been reported by Braddock and Meyer (*J. Am. Chem. Soc.* **1973**, *95*, 3158$-$3162). While negative ΔH^* values have not been observed here, we note that the predicted absolute magnitudes of the negative activation enthalpies are small (see Figure 8).

(68) Using the 1600 cm^{-1} mode in the nonclassical activation enthalpy calculations produces similar results: an activation enthalpy of 8 kJ mol^{-1} was calculated assuming an entropic driving force of -192 J deg^{-1} mol^{-1}, an activation enthalpy of 5 kJ mol^{-1} for $\Delta S = -96$ J deg^{-1} mol^{-1}, but only 2 kJ mol^{-1} assuming $\Delta S = 0$.